Size-Dependent Properties of Multiferroic $BiFeO_3$ Nanoparticles

Sverre M. Selbach,[†] Thomas Tybell,[‡,§] Mari-Ann Einarsrud,[†] and Tor Grande[†,*]

Department of Materials Science and Engineering, Department of Electronics and Telecommunications, and NTNU Nanolab, Norwegian University of Science and Technology, 7491 Trondheim, Norway

Received July 11, 2007. Revised Manuscript Received September 24, 2007

$BiFeO_3$ nanoparticles prepared by a modified Pechini method display strong size-dependent properties. The rhombohedral distortion from cubic structure is reduced by decreasing particle size accompanied by decreasing polarization inferred from atomic displacements found by Rietveld refinement of X-ray powder diffraction data. With decreasing crystallite size, the Néel temperature decreased and the magnetic transition was increasingly diffuse. The Néel temperature was shown to correlate with the volume of the crystallites and the polar displacements of cations.

Introduction

Multiferroics[1,2] with significant magnetoelectric[3] coupling opens exciting opportunities for designing microelectronic devices with control of magnetic domains by electric fields[4] or vice versa.[5] Magnetoelectric $BiFeO_3$ has received considerable attention the past few years because of its potential applications[6,7] in data storage, sensors, filters, attenuators and devices for spintronics, and reports of enhanced polarization in epitaxially strained thin films.[8,9] $BiFeO_3$ display coexistence of ferroelectricity ($T_{C,bulk} = 826–45$ °C)[10–12] and antiferromagnetism ($T_{N,bulk} = 370$ °C)[13] over a wide temperature range above room temperature. $BiFeO_3$ is a rhombohedrally distorted perovskite belonging to the space group $R3c$ with rhombohedral lattice parameters $a_r = 5.63$ Å, $\alpha_r = 59.35°$, or alternatively, hexagonal parameters $a_{hex} = 5.58$ Å, $c_{hex} = 13.87$ Å.[13–15] The antiferromagnetic ordering in bulk $BiFeO_3$ is G-type below T_N.[12] A canted spin structure gives a spiral modulation with a periodicity of 62 nm, incommensurate with the crystal lattice.[16] So far, the majority of reports on $BiFeO_3$ are on thin films, where epitaxial strain is shown to influence the observed properties such as crystal structure, polarization, and magnetization.[8,9,17] Corresponding characterization of $BiFeO_3$ nanoparticles, which would give the size-dependent properties without the influence of strain induced by a substrate, is scarce. The Néel temperature T_N of $BiFeO_3$ has been shown to decrease with decreasing particle size.[18] Enhanced magnetization in small particles has recently been reported and attributed to surface-induced magnetization[19] and ferromagnetism caused by apparent oxygen deficiency.[20] No evident trends in lattice parameters with particle size were reported by Shetty et al.[18] The influence of finite size on lattice parameters and polar displacements of atoms will provide insight to the finite size effects on ferroelectricity. We have characterized $BiFeO_3$ nanocrystallites by X-ray diffraction (XRD) to investigate the size-dependent structural properties and correlated the structural data with size-dependent T_N measured by differential scanning calorimetry (DSC).

Experimental Section

$BiFeO_3$ nanocrystallites were prepared by a modified Pechini method using nitrates as metal precursors.[21] The precursors were prepared by dissolving $Bi(NO_3)_3 \cdot 5\ H_2O$ (Fluka, >99%) and $Fe(NO_3)_3$ (Merck, >99%) in distilled water with the addition of HNO_3 (Merck, 65%) to pH 1–2. The concentrations of metal cations in the nitrate solutions were determined by thermogravimetrical

---

[*] To whom correspondence should be addressed. E-mail: tor.grande@material.ntnu.no.

[†] Department of Materials Science and Engineering, Norwegian University of Science and Technology.

[‡] Department of Electronics and Telecommunications, Norwegian University of Science and Technology.

[§] NTNU Nanolab, Norwegian University of Science and Technology.

(1) Smolenskii, G. A.; Chupis, I. E. *Sov. Phys. Usp.* **1982**, *25*, 475–493.
(2) Eerenstein, W.; Mathur, N. D.; Scott, J. F. *Nature* **2006**, *442*, 759–765.
(3) Fiebig, M. *J. Phys. D: Appl. Phys.* **2005**, *38*, R123–152.
(4) Lottermoser, Th.; Lonkal, T.; Amann, U.; Hohlwein, D.; Ihringer, J.; Fiebig, M. *Nature* **2004**, *430*, 541–544.
(5) Kimura, T.; Goto, T.; Shintani, H.; Ishizaka, K.; Arima, T.; Tokura, Y. *Nature* **2003**, *426*, 55–58.
(6) Spaldin, N. A.; Fiebig, M. *Science* **2005**, *309*, 391–392.
(7) Ramesh, R.; Spaldin, N. A. *Nat. Mater.* **2007**, *6*, 21–29.
(8) Wang, J.; Neaton, J. B.; Zheng, H.; Nagarajan, V.; Ogale, S. B.; Liu, B.; Viehland, D.; Vaithyanathan, V.; Schlom, D. G.; Waghmare, U. V.; Spaldin, N. A.; Rabe, K. M.; Wuttig, M.; Ramesh, R. *Science* **2003**, *299*, 1719–1722.
(9) Yun, K. Y.; Ricinschi, D.; Kanashima, T.; Noda, M.; Okuyama, M. *Jpn. J. Appl. Phys.* **2004**, *43*, L647–L648.
(10) Bucci, J. D.; Robertson, B. K.; James, W. D. *J. Appl. Crystallogr.* **1972**, *5*, 187–191.
(11) Mahesh Kumar, M.; Palkar, V. R.; Srinivas, K.; Suryanarayana, S. V. *Appl. Phys. Lett.* **2000**, *76*, 2764–2766.
(12) Maître, A.; François, M.; Gachon, J. C. *J. Phase Equilib.* **2004**, *25*, 59–67.
(13) Moreau, J. M.; Michel, C.; Gerson, R.; James, W. J. *J. Phys. Chem. Solids* **1971**, *32*, 1315–1320.
(14) Kubel, F.; Schmid, H. *Acta Crystallogr., Sect. B* **1990**, *46*, 698–702.
(15) Fischer, P.; Polomska, M.; Sosnowska, I.; Szymanski, M. *J. Phys. C: Solid. State Phys.* **1980**, *13*, 1931–1940.
(16) Sosnowska, I.; Peterlin-Neumaier, T.; Steichele, E. *J. Phys. C: Solid State Phys.* **1982**, *15*, 4835–4846.
(17) Jiang, Q.; Qiu, J. H. *J. Appl. Phys.* **2006**, *99*, 103901.
(18) Shetty, S.; Palkar, V. R.; Pinto, R. *Pramana* **2002**, *58*, 1027–1030.
(19) Park, T.-J.; Papaefthymiou, G. C.; Viescas, A. J.; Moodenbaugh, A. R.; Wong, S. S. *Nano Lett.* **2007**, *7*, 766–772.
(20) Mazumder, R.; Sujatha Devi, P.; Bhattacharya, D.; Choudhury, P.; Sen, A.; Raja, M. *Appl. Phys. Lett.* **2007**, *91*, 062510.
(21) Selbach, S. M.; Tybell, T.; Einarsrud, M.-A.; Grande, T. *J. Am. Ceram. Soc.* **2007**, *90*, 2649–2652.

10.1021/cm071827w CCC: $37.00

Table 1. Calcination Temperature, Size, and Lattice Parameters

		unit-cell parameter		
T (°C)[a]	size d (nm)	a_{hex}(Å)	c_{hex}(Å)	T_{N} (°C)
400	11.0 ± 2	5.59(36)	13.8(19)	
410	13.0 ± 1	5.585(55)	13.83(88)	355 ± 7
425	13.3 ± 1	5.587(87)	13.84(17)	360.7 ± 5.5
450	15.3 ± 1	5.585(66)	13.84(60)	363.3 ± 4
500	20.4 ± 2	5.580(67)	13.852(42)	371.1 ± 3
500[b]	29.6 ± 5	5.578(53)	13.860(10)	371.8 ± 2.5
550	34.4 ± 6	5.578(26)	13.859(46)	375.4 ± 2.5
575	38.0 ± 7	5.577(99)	13.860(20)	
600[c]	50.7 ± 10	5.577(29)	13.864(02)	375.8 ± 2
587[b]	52.1 ± 11	5.576(92)	13.864(40)	
600[d]	61.5 ± 14	5.577(49)	13.865(53)	376.6 ± 2
600	72.1 ± 18	5.5775(23)	13.863(14)	379.7 ± 2
650[b]	86.4 ± 23	5.5770(8)	13.864(87)	
bulk		5.5772(04)	13.865(75)	378.0 ± 2

[a] Unmarked syntheses (calcd temp) were done with maleic and ethylene glycol (EG). [b] Syntheses were done with malic acid without EG. [c] Syntheses were done with tartaric acid without EG. [d] Syntheses were done with malic acid and EG.

analysis to be 0.317 and 1.628 mmol g^{-1} for bismuth and iron, respectively. The carboxylic acids used were DL-tartaric acid (Acros Organics, 99.5%), DL-malic acid (Aldrich, 99%), and maleic acid (Merck, >99%). Carboxylic acid (0.03 mol) was dissolved in distilled water (30 mL). Metal nitrate precursor solutions (0.015 mol of each) were mixed and added to the carboxylic acid under stirring. Ethylene glycol (Acros Organics, >99.9%) (EG) in a molar ratio to the respective carboxylic acid of 1:1 was finally added to some of the syntheses as a polymerizing agent. The majority of the materials were prepared with maleic acid and EG. Materials labeled *b* and *c* in Table 1 were prepared with DL-tartaric acid and DL-malic acid, respectively, without EG. The material labeled *d* was prepared with DL-malic acid and EG. The solutions were evaporated into dry polyester precursors. Grinded precursor powders were calcined in air with a heating rate of 400 °C h^{-1} and a soaking time of 2 h at temperatures from 400 to 650 °C. Bulk $BiFeO_3$ was made by traditional solid-state reaction of Bi_2O_3 (Aldrich, >99.9%) and Fe_2O_3 (Merck, >99%). Dried starting materials were mixed by ball milling in ethanol for 24 h using yttria-stabilized zirconia balls. Pellets were fired once at 825 °C for 8 h with a 400 °C h^{-1} heating and cooling rate; the term "bulk" refers to this material.

XRD characterization at room temperature was performed on a $\theta-\theta$ Bruker AXS D8 ADVANCE (Karlsruhe, Germany) diffractometer with a VANTEC-1 detector and Cu Kα radiation. Data were collected using a 0.016° step size and 1 s count time over the 2θ range 20−90°. The crystallite sizes (d_{XRD}) were calculated from the $(024)_{\mathrm{hex}}$ Bragg reflections by the Scherrer equation corrected for instrumental peak broadening determined with a LaB_6 standard. The particle size of the powders is taken to correspond to the crystallite size in the following. High-temperature XRD (HTXRD) up to 400 °C on bulk powder was performed with a Siemens D5005 $\theta-\theta$ diffractometer using Cu Kα radiation and a position-sensitive monochromator. The powder was dispersed in ethanol and applied on a platinum strip located in a high-temperature camera (HTK 16, Anton Paar, GMbh). High-temperature measurements were performed in air from 20 to 100° with a count time of 3 s per step and a step size of 0.036°. Prior to each scan, the powder was held for 30 min at the temperature to establish thermal equilibrium.

The software TOPAS R (Bruker AXS, version 2.1) was used for Rietveld refinements. The space group $R3c$ in its hexagonal representation was used as the basis, and the starting values for all Rietveld refinements were $a_{\mathrm{hex}} = 5.577$ Å, $c_{\mathrm{hex}} = 13.86$ Å, Bi (0,0,0.2988), Fe (0,0,0.197), O (0.2380,0.3506,1/12).[15] The background was refined using a fifth-order Chebichev function for all patterns, except the one of the smallest crystallites, where a higher-order function was necessary to fit the amorphous background. A Pearson VII function was used to fit the peak shape. Displacement was refined and zero error was fixed at a value obtained from a LaB_6 standard. Lattice parameters, peak shape, background, and displacement were refined simultaneously; atomic positions were consecutively added to the refinement after convergence, starting with the heavier atoms. Isotropic temperature factors B were fixed during the refinement as 1.03, 0.76, and 0.89 Å^2 for Bi, Fe, and O,[22] respectively, for the room-temperature data, and refined for high-temperature data. All relevant parameters from the refinements of room-temperature patterns of nanocrystallites are given in the Supporting Information.

Transmission electron microscopy (TEM) was performed using a JEM 2010 microscope with a point-to-point resolution of 0.23 nm. The microscope was equipped with an energy-dispersive X-ray spectroscopic (EDS) detector, operated at an accelerating voltage of 200 kV. Powder calcined at 450 °C for 2 h was ball-milled for 1 h in ethanol before the powder was finally retrieved on a holy carbon grid for high-resolution TEM observations.

Differential scanning calorimetry (DSC) was performed with a Perkin-Elmer DSC 7, PE thermal analysis controller TAC 7/DX, and Pyris version 3.81 software. Samples of 20–50 mg were encapsulated in aluminum sample pans, and the measurements were done with 40 °C min^{-1} heating and cooling rates in the temperature region 25–550 °C.

Thermogravimetrical analysis was performed with a Netzsch STA 449 C *Jupiter* in synthetic air on two powder samples heat-treated for 2 h at 425 and 500 °C, with initial crystallite size of 13.3 ± 1 and 20.4 ± 2 nm, respectively. The samples were heated to 400 °C with a rate of 10 °C min^{-1}, held for 8 h to remove adsorbed water, and further heated to 600 °C at the same rate and held for 8 h to measure mass loss/gain due to reduction/oxidation during crystallite growth.

Results and Discussion

XRD patterns of the as-prepared powders annealed for 2 h at temperatures from 400 to 650 °C confirmed that the materials were phase-pure $BiFeO_3$ belonging to the space group $R3c$ (JCPDS 86-1518; see Figure S1 in the Supporting Information). Careful characterization of the concentration of Fe and Bi in the precursor solutions was performed to ensure that stoichiometric materials, and no secondary phases, observed by solid-state synthesis of $BiFeO_3$ because of offset from the nominal stoichiometry,[21] could be detected.

The possible oxygen nonstoichiometry of the nanocrystalline powders was studied by thermogravimetry. Unfortunately, the volatile suboxide BiO(g)[22] hinders direct determination of the absolute oxygen stoichiometry by in situ reduction, but relative change in the oxygen content during coarsening of the nanocrystalline powders could be determined by thermogravimetry. Only negligible weight change of the powders was observed during coarsening of powders (preheated at 400 °C) at 600 °C for 8 h with initial size of 13.3 ± 1 and 20.4 ± 2 nm. The final crystallite size of the powders after the annealing process was 100 ± 20 nm, and the relative weight change during the isothermal annealing corresponds to a change in oxygen stoichiometry of less than 0.01. On the basis of these data, we propose that there is no finite size effect on the oxidation state of Fe in the powders.

---

(22) Onyama, E.; Wahlbeck, P. G. *J. Phys. Chem. B* **1998**, *102*, 4418–4425.

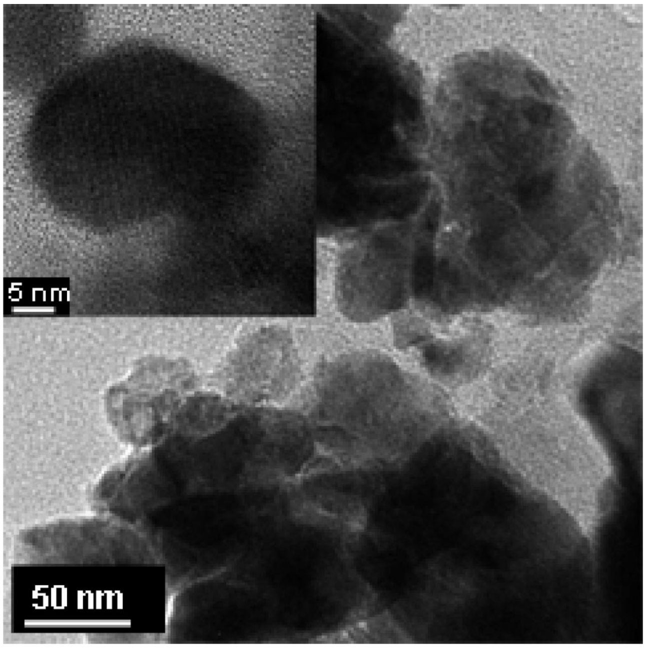

Figure 1. Transmission electron micrograph of powder calcined for 2 h at 450 °C, showing nanocrystallites in agglomerates. Inset shows dimensions and morphology of a typical individual nanocrystallite.

Table 2. Atomic Positions in the Hexagonal Unit Cell

	x	*y*	*z*
Bi^{3+}	0	0	$¼ + s$
Fe^{3+}	0	0	t
O^{2-}	$1/6 - 2e - 2d$	$1/3 - 4d$	1/12

This is also reasonable because significant reduction in the partial pressure of oxygen (1×10^{-15} to 1×10^{-20} bar) is necessary to make Fe^{2+} stable in this temperature range.[23]

The mean crystallite sizes of the powders, determined by the Scherrer equation, and their thermal history are summarized in Table 1. We have previously shown that calculated particle size from surface area measurements are in reasonable agreement with the crystallite size obtained by the Scherrer equation.[21] Additional support was obtained by TEM characterization, and typical morphology of particle agglomerates and an individual nanocrystallite are shown in Figure 1. The TEM image and surface area measurements demonstrate that the crystallite size obtained by the Scherrer equation is slightly smaller than the particle size because of agglomeration of the particles (see Figure 1). We therefore conclude that the crystallite size found by the Scherrer equation is a reasonable estimate for the particle size.

We have adopted the representation of the atomic positions in the hexagonal unit cell provided by Megaw and Darlington.[26] Coordinates for all the atoms in the unit cell as a function of the displacement parameters s, t, d, and e are given in Table 2. The z coordinate of the oxygen atom is fixed in this representation. The crystallographic displacement of Bi^{3+} and Fe^{3+} in $BiFeO_3$ is illustrated in Figure 2. The parameters s and t describe the polar displacements of Bi^{3+} and Fe^{3+} from their positions defined by $s = 0$ and $t = 0$ corresponding to a nonpolar space group with inversion symmetry.[26] Displacements s and t are parallel to the polar [111] axis of the rhombohedral unit cell,[27] which is parallel to the hexagonal [001] axis. The oxygen position parameter d is related to the distortion of the FeO_6 octahedra parallel to the $[001]_{hex}$ axis, whereas the parameter e is linked to the antiferrodistortive rotation of the octahedra by the angle Φ about the $[001]_{hex}$ axis by $2e\sqrt{3} = \tan \Phi$, $e = 0$ and $d \neq 0$ ($s \neq 0$ and $t \neq 0$) correspond to atomic positions in the polar space group $R3m$, whereas $d = 0$ and $e \neq 0$ ($s = 0$ and $t = 0$) correspond to the centrosymmetric space group $R\bar{3}c$.[26] The octahedral strain parameter $\eta = c_{hex}\cos \Phi / a_{hex}\sqrt{6}$ has the values $\eta = 1$, $\eta < 1$, and $\eta > 1$ for regular, compressed, and elongated oxygen octahedra along the $[001]_{hex}$ axis, respectively.[26,28] The scaling of Φ with size, obtained from the oxygen x and y positions, did not yield any evident trend, whereas η is <1 for bulk and decreases with crystallite size (see the Supporting Information).

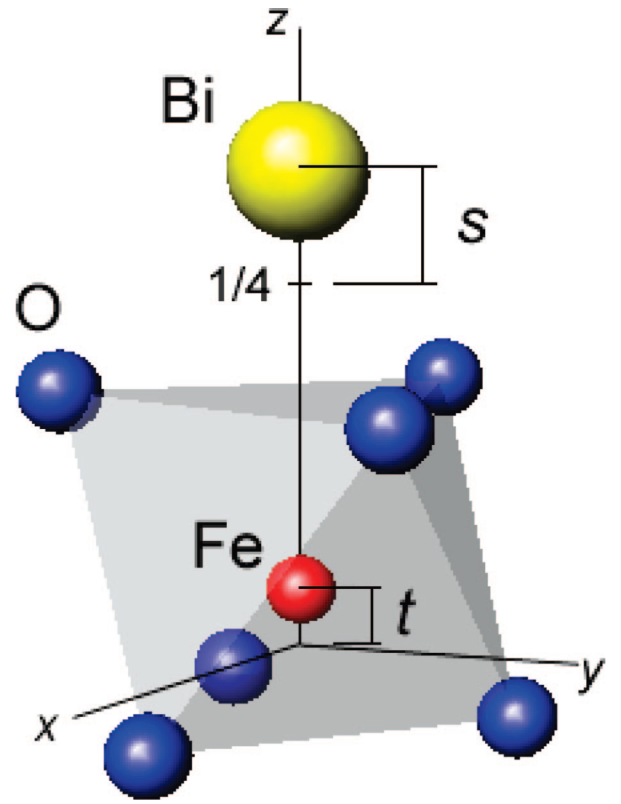

Figure 2. Displacements s and t of Bi^{3+} and Fe^{3+}, respectively, along the hexagonal [001] axis. $s > t$ and $(s - t)$ is a crystallographic measure of polarization. $s = 0$ and $t = 0$ correspond to $z = 0$ and ¼, respectively, as in a nonpolar space group. Spontaneous polarization P_s is parallel to the [001] axis, antiferrodistortive rotation of the oxygen octahedron is about the [001] axis.

The lattice parameters obtained by the Rietveld refinement are summarized in Table 1. The normalized lattice parameters $a = a_{hex}/\sqrt{2}$ and $c = c_{hex}/\sqrt{12}$ are shown as a function of crystallite size, along with the pseudotetragonality c/a in

---

[23] Darken, L. S.; Gurry, R. W. *J. Am. Chem. Soc.* **1946**, *68*, 798–816.
[24] Sosnowska, I.; Schäfer, W.; Kockelmann, W.; Andersen, K. H.; Troyanchuk, I. O. *Appl. Phys. A: Mater. Sci. Process.* **2002**, *74*, S1040–S1042.
[25] Rietveld, H. M. *J. Appl. Crystallogr.* **1969**, *2*, 65–71.
[26] Megaw, H. D.; Darlington, C. N. W. *Acta Crystallogr., Sect. A* **1975**, *31*, 161–173.
[27] Michel, C.; Moreau, J. M.; Achenbach, G. D.; Gerson, R.; James, W. J. *J. Solid State Commun.* **1969**, *7*, 701–704.
[28] Thomas, N. W. *Acta Crystallogr., Sect. B* **1996**, *52*, 954–960.

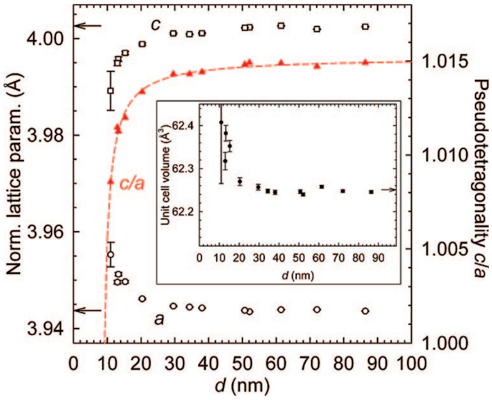

Figure 3. Normalized lattice parameters *a* (open circles), *c* (open squares), and pseudotetragonality *c*/*a* (filled triangles) of nanocrystalline $BiFeO_3$ as a function of crystallite size *d*. Arrows denote bulk values. The dashed line is a fit to eq 1 for *c*/*a*, extrapolation indicates a critical size of 9 ± 1 nm. Inset: primitive unit-cell volume versus crystallite size.

Figure 3. Crystallites larger than 30 nm display bulk lattice parameters. Below 30 nm, the lattice parameters deviate from bulk, approaching a cubic perovskite structure with decreasing particle size, corresponding to the normalized lattice parameters becoming equal. Decreasing rhombohedral distortion of the unit cell with decreasing crystallite size is reflected in the reduction in *c*/*a*, which becomes equal to unity when the rhombohedral angle becomes 60°, corresponding to an ideal, cubic perovskite. The primitive unit-cell volume versus the crystallite size is shown in the inset in Figure 3. The unit-cell volume does not deviate from the bulk value for crystallites larger than 30 nm and increases with reduction in the crystallite size below 30 nm. The increase in unit-cell volume observed is typical for partly covalent oxides.[29] Finite size effects on the lattice parameters of $BiFeO_3$ become pronounced at significantly smaller crystallite size (below 30 nm) than for the prototype ferroelectrics $PbTiO_3$ (below 50–150 nm)[30–33] and $BaTiO_3$ (below 0.15–1 μm).[34–36] These two materials, which display a Curie temperature considerably lower than for $BiFeO_3$, are tetragonal perovskites and become cubic in the paraelectric state. For $PbTiO_3$ and $BaTiO_3$, the tetragonal distortion from ideality, $c/a - 1$, is a crystallographic order parameter for the ferroelectric phase transition, and the critical size for the existence of ferroelectricity in nanoparticles of these two materials have been reported at 7–15[30–33,37,38] and 70–120 nm,[34–36,39,40] respectively. We observe the ferroelectric phase of $BiFeO_3$ for smaller crystallites than the critical size for $BaTiO_3$ and for most estimates for $PbTiO_3$. Ishikawa et al.[32] have fitted the size-dependent tetragonality of $PbTiO_3$ to the empirical model

$$\left(\frac{c}{a}\right)_{\mathrm{d}} = \left(\frac{c}{a}\right)_{\infty} - \frac{A}{d - d_{\mathrm{c}}} \qquad (1)$$

where $(c/a)_{\mathrm{d}}$ is the size-dependent tetragonality, $(c/a)_\infty$ the bulk tetragonality, *A* a fitting parameter, and d_c a fitting parameter close to the critical size for ferroelectricity. Fitting our normalized lattice parameters to eq 1 yields $d_c = 9 \pm 1$ nm (Figure 3). When comparing $BiFeO_3$ to the prototype ferroelectrics $PbTiO_3$ and $BaTiO_3$, a high ferroelectric T_C is accompanied by a small critical size of ferroelectricity and bulk lattice parameters prevailing to smaller crystallite sizes.

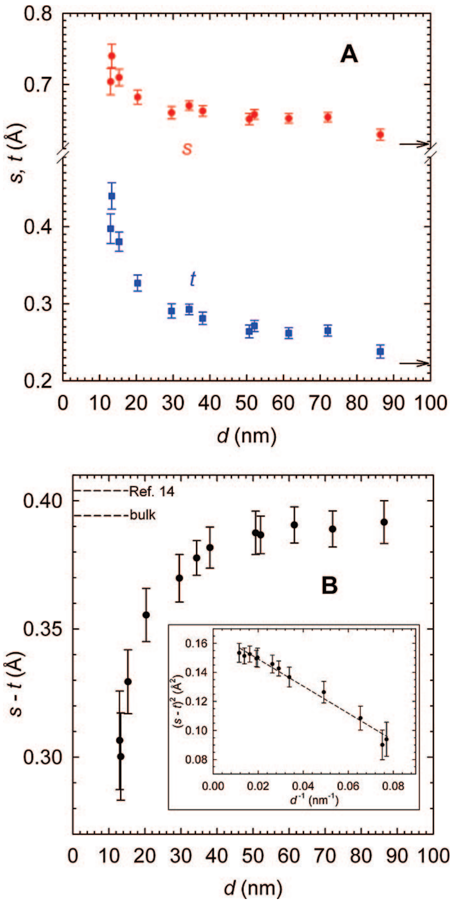

Figure 4. (A) Displacements of Bi^{3+} and Fe^{3+} expressed as *s* and *t*, arrows denote bulk values. (B) Relative displacements of Bi^{3+} and Fe^{3+} expressed as $s - t$, dashed lines denote values for bulk powder and single crystal.[14] Inset in (B) $(s - t)^2$ decreases linearly with inverse crystallite size; the dashed line is a guide to the eye.

Crystallographic displacement of Bi^{3+} and Fe^{3+} from the nonpolar positions are shown as a function of the crystallite size in Figure 4A. When *t* approaches *s*, the cation sublattices become more regular, as $s = t$ would correspond to an equally spaced array of cations.[26] Note that the displacements

---

(29) Ayyub, P.; Palkar, V. R.; Chattopadhyay, S.; Multani, M. *Phys. Rev. B* **1995**, *51*, 6135–6138.

(30) Zhong, W. L.; Jiang, B.; Zhang, P. L.; Ma., J. M.; Cheng, H. M.; Yang, Z. H.; Li, L. X. *J. Phys.: Condens. Matter* **1993**, *5*, 2619–2624.

(31) Chattopadhyay, S.; Ayyub, P.; Palkar, V. R.; Multani, M. *Phys. Rev. B* **1995**, *52*, 13177–13183.

(32) Ishikawa, K.; Nomura, T.; Okada, N.; Takada, K. *Jpn. J. Appl. Phys.* **1996**, *35*, 5196–5198.

(33) Akdogan, E. K.; Rawn, C. J.; Porter, W. D.; Payzant, E. A.; Safari, A. *J. Appl. Phys.* **2005**, *97*, 084305.

(34) Uchino, K.; Sadanaga, E.; Hirose, T. *J. Am. Ceram. Soc.* **1989**, *72*, 1555–1558.

(35) Yamamoto, T.; Urabe, K.; Banno, H. *Jpn. J. Appl. Phys.* **1993**, *32*, 4272–4276.

(36) Yan, T.; Shen, Z.-G.; Zhang, W.-W.; Chen, J.-F. *Mater. Chem. Phys.* **2006**, *98*, 450–455.

(37) Ishikawa, K.; Yoshikawa, K.; Okada, N. *Phys. Rev. B* **1988**, *37*, 5852–5855.

(38) Erdem, E.; Semmelhack, H.-C.; Böttcher, R.; Rumpf, H.; Banys, J.; Matthes, A.; Gläsel, H.-J.; Hirsch, D.; Hartmann, E. *J. Phys.: Condens. Matter* **2006**, *18*, 3861–3874.

(39) Akdogan, E. K.; Safari, A. *Jpn. J. Appl. Phys.* **2002**, *41*, 7170–7175.

(40) Tsunekawa, S.; Ito, S.; Mori, T.; Ishikawa, K.; Li, Z.-Q.; Kawazoe, Y. *Phys. Rev. B* **2000**, *62*, 3065–3070.

of Bi^{3+} and Fe^{3+} do not approach the nonpolar positions. t and s change from 0.016(06) (0.222(68) Å) and 0.044(48) (0.616(75) Å), respectively, for bulk to 0.02(87) (0.39(75) Å) and 0.05(09) (0.70(40) Å), respectively, for the smallest crystallites. We propose the crystallographic parameter $s - t$ as an appropriate measure of the spontaneous polarization in $BiFeO_3$. In $BiFeO_3$, the main source of spontaneous polarization is the displacement of Bi^{3+} caused by the stereochemically active 6 s^2 lone pair.[41] Covalent bonding between the 6 s^2 lone pair of Bi^{3+} and O^{2-} 2p orbitals has also recently been confirmed theoretically,[42] as well as between Fe^{3+} and O^{2-}. First-principles studies by Ravindran and co-workers[42] indicate that the displacement of Bi^{3+} is responsible for approximately 98.5% of the total spontaneous polarization. The partial polarizations caused by displacements of Bi^{3+} and Fe^{3+} almost cancel each other out, and the net polarization is mainly in the direction of $[001]_{\text{hex}}$ because of the relative displacement of the two cations along this direction. First-principles calculations thus provide a sound theoretical basis for our choise of $s - t$ as a crystallographic measure of polarization. The relative displacement of the cations, $s - t$, is equal to Δz_{hex} of Fe^{3+} with Bi^{3+} fixed at $z = 0$. The rhombohedral, ferroelectric perovskites $LiNbO_3$ and $LiTaO_3$, isomorphous with $BiFeO_3$, both show a linear relation between Δz of Nb/Ta cation and the spontaneous polarization, quantified empirically[43] by $P_S = (258 \pm 9)\,\Delta z$ μC cm^{-2}. For $BiFeO_3$, this relation predicts bulk P_S to be 98–108 μC cm^{-2}, in reasonable agreement with first-principles predictions of 90–100 μC cm^{-2}[40] and 88.7 μC cm^{-2}.[41] The relative displacements of the two cations demonstrate a clear dependence of size, and $s - t$ reduces with approximately 25% from bulk to 13 nm, Figure 4B. The depolarization energy E_d of a ferroelectric nanoparticle scales with squared polarization P^2 and inverse size,[44] $E_d \propto P^2 d$. P^2, represented by $(s - t)^2$, scales linearly with d^{-1} (Figure 4B, inset). Hence, the increase in deviation of $s - t$ from bulk value with decreasing crystallite size is likely to be caused by an increase in depolarization field. The finite size effects on pseudotetragonality and polar displacements of cations show different behavior. We note that the parameter $s - t$ deviates from bulk value in crystallites larger than 30 nm, where lattice parameters are equal to bulk. This indicates an onset of a reduced polarization before the pseudotetragonality is affected. Even at 13 nm, $s - t$ has a significant finite value, approximately 75% of bulk, which is a promising result regarding the possibility of making small nanostructures with sufficient polarization for technological applications.

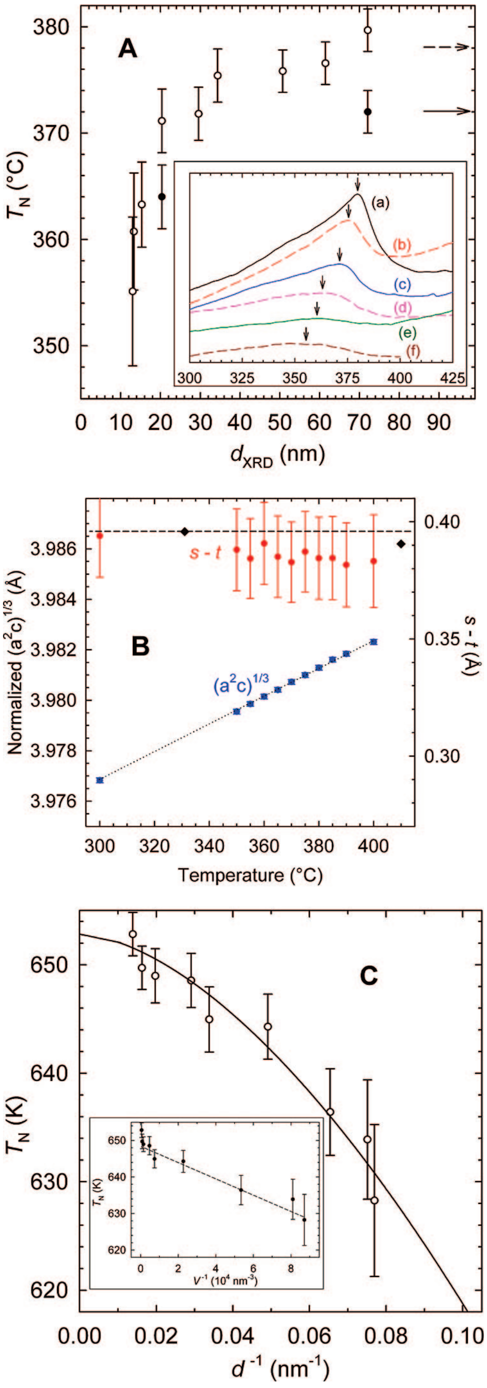

Figure 5. (A) Néel temperatures of nanocrystalline $BiFeO_3$ as a function of crystallite size; open circles are measured with a heating rate of 40 °C min^{-1}, filled circles with 10 °C min^{-1} for comparison. Solid and dashed arrows denote bulk values measured at 10 and 40 °C min^{-1}, respectively. Inset in (A): DSC traces of selected materials measured at 40 °C min^{-1}. (a) Bulk, (b) 72.1, (c) 34.4, (d) 20.4, (e) 15.3, (f) 13.3, and (g) 13.0 nm, arrows denote peak position and T_N. (B) Normalized mean lattice parameter $(a^2c)^{1/3}$ and the crystallographic quantity $s - t$ for bulk $BiFeO_3$ in the temperature interval of the antiferromagnetic to paramagnetic phase transition. The dashed line is the room temperature value of $s - t$ for bulk powder, filled diamonds are values adopted from ref 15 and the dotted line is a guide to the eye. (C) T_N measured at 40 °C min^{-1} vs d^{-1}, fitting to eq 2 gives $\nu = 0.6 \pm 0.1$ and $d_0 = 1.7 \pm 0.5$ nm. Inset: T_N is proportional to the inverse crystallite volume; the dashed line is a guide to the eye.

The antiferromagnetic to paramagnetic transition of $BiFeO_3$ nanocrystallites was measured by DSC. T_N vs crystallite size is shown in Figure 5A. The transition temperatures, summarized in Table 1, were defined as the peak position of the DSC curves by numerical differentiation, see inset Figure 5A. Below ~50 nm T_N decreases significantly below the bulk value. The calorimetric peaks become increasingly diffuse with decreasing crystallite size (inset

---

(41) Neaton, J. B.; Ederer, C.; Waghmare, U. V.; Spaldin, N. A.; Rabe, K. M. *Phys. Rev. B* **2005**, *71*, 014113.

(42) Ravindran, P.; Vidya, R.; Kjekshus, A.; Fjellvåg, H.; Eriksson, O. *Phys. Rev. B* **2006**, *74*, 224412.

(43) Abrahams, S. C.; Kurtz, S. K.; Jamieson, P. B. *Phys. Rev.* **1968**, *172*, 551–553.

(44) Shih, W. Y.; Shih, W.-H.; Aksay, I. A *Phys. Rev. B* **1994**, *50*, 15575–15585.

Figure 5A). To increase the sensitivity (heat flow) of the DSC instrument, the heating rate used was 40 °C/min, accounting for the small difference in measured bulk T_N of 378 °C and the literature value of 370 °C.[13,45] Despite the shift in T_N due to the heating rate, we propose that the relative change in T_N with particle size would not be influenced by the heating rate. T_N equal to 360 °C has recently reported by Mazumder et al. for a 40 nm particle size.[20] The discrepancy between this value and the present data is mainly attributable to the shift in our data due to the high heating rate used for DSC, but the difference in synthesis route may also be important because Mazumder et al. measured on apparently oxygen-non-stoichiometric powders also containing traces of other phases. Results from HTXRD measurements on bulk BiFeO$_3$ in Figure 5B did not reveal any unit-cell volume change associated with the magnetic transition in contradiction with previous reports.[10,15] No abrupt structural changes in the crystallographic data could be associated with the magnetic transition. The findings from DSC and HTXRD measurements in the vicinity of T_N, combined with a reported singularity in $d(\Delta V/V)/dT$ at T_N[46] and not a discontinuity in volume, demonstrate the magnetic phase transition to be second order, in contradiction with previous claims that it is first order.[20,46]

A finite size-dependent magnetic ordering temperature of a ferro-, ferri-, or antiferromagnetic material can be described by the phenomenological scaling relation[47,48]

$$\frac{T_N(d) - T_N(\infty)}{T_N(\infty)} = \pm\left(\frac{d}{d_0}\right)^{-1/\nu} \qquad (2)$$

where $T_N(\infty)$ is the bulk T_N, $T_N(d)$ the size-dependent T_N, d the crystallite size, d_0 the characteristic microscopic length of the system, and ν the correlation length exponent. A least-squares fit yields values of $\nu = 0.6 \pm 0.1$ and $d_0 = 1.7 \pm 0.5$ nm, Figure 5C. A correlation length exponent of 0.5 would correspond to the theoretical critical exponent for a mean field behavior, whereas 0.7 would correspond to a 3D Heisenberg model.[48,49]

The magnetic transition temperature T_N scales linearly with the inverse volume V^{-1} in the size region where T_N decreases, inset Figure 5C. Ignoring possible magnetoelectric influence of polarization on the magnetic ordering, the inverse volume dependence of T_N indicates that the ordering temperature is proportional to the number of antiferromagnetic exchange interactions in a certain size region larger than the magnetic correlation volume. Below this critical volume, the ordering completely disappears, whereas bulk T_N prevails for particles larger than approximately 50 nm. XAFS studies of bulk and 20 nm particles of BiFeO$_3$ indicate that the decrease in T_N is not due to local structural changes about Fe^{3+}.[50]

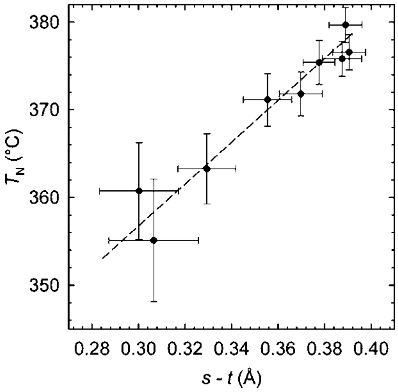

Figure 6. Comparing $s - t$ and T_N for the same crystallite sizes yields a linear relationship; the dashed line is a guide to the eye.

Finally, we discuss possible correlations between the observed finite size effects on the structural properties and the Néel temperature T_N. Antiferromagnetic domains can be controlled by electric-field-induced switching of ferroelastic domains, and antiferromagnetic planes in BiFeO$_3$ are perpendicular to the polar axis,[51] hence their stability may be influenced by the magnitude of the polarization. The linear decrease in $(s - t)^2$ with inverse crystallite size (inset, Figure 4B) and the linear decrease in T_N with inverse crystallite volume (inset, Figure 5C) have already been pointed out. Within the temperature interval in question for T_N, 300−400 °C, $s - t$ is close to room-temperature values (Figure 5C), compared to the substantial influence of finite size on $s - t$ (Figure 4B). By comparing T_N and $s - t$ for the same materials, we observe that the decrease in T_N scales linearly with the decrease in $s - t$, Figure 6. The antiferromagnetic ordering may thus be influenced by the polarization and possibly stabilized. The decrease in T_N observed could be associated with the decrease in spontaneous polarization quantified by $s - t$, in addition to the decrease in the number of antiferromagnetic interactions with decreasing particle volume. This is in agreement with related findings of dielectric and phonon anomalies at T_N. A dielectric anomaly occurs at T_N in BiFeO$_3$,[52] and phonon anomalies at T_N in BiFeO$_3$ are an order of magnitude larger than in the related antiferromagnetic, nonferroelectric compound EuFeO$_3$.[53] Size-dependent softening[19] of the A1 (TO) mode, corresponding to the out-of-phase vibrations of Bi^{3+} and FeO$_6$ octahedra,[54,55] has been reported. Moreover, an imbalance of the Mn^{3+}−R^{3+} superexchange induced by ferroelectric distortion is shown to be the microscopic origin of the magnetoelectric effect in multiferroic rear earth manganites.[56] There are thus several observations suggesting a correlation between size-dependent ferroelectric and antiferromagnetic

---

(45) In separate experiments with a lower heating rate of 10 K/min, bulk T_N was found to be in excellent accordance with previous reports.

(46) Mazumder, R.; Ghosh, S.; Mondal, P.; Bhattacharya, D.; Dasgupta, S.; Das, N.; Sen, A.; Tyagi, A. K.; Sivakumar, M.; Takami, T.; Ikuta, H. *J. Appl. Phys.* **2006**, *100*, 033908.

(47) Landau, D. P. *Phys. Rev. B* **1976**, *14*, 255–262.

(48) Batlle, X.; Labarta, A. *J. Phys. D.: Appl. Phys.* **2002**, *35*, R15–R42.

(49) Chaikin, P. M.; Lubensky, T. C. *Principles of Condensed Matter Physics*; Cambridge University Press: Cambridge, U.K., 1995.

(50) Chattopadhyay, S.; Kelly, S. D.; Palkar, V. R.; Fan, L.; Segre, C. U. *Phys. Scr.* **2005**, *T115*, 709–713.

(51) Zhao, T.; Scholl, A.; Zavaliche, F.; Lee, K.; Barry, M.; Doran, A.; Cruz, M. P.; Chu, Y. H.; Ederer, C.; Spaldin, N. A.; Das, R. R.; Kim, D. M.; Baek, S. H.; Eom, C. B.; Ramesh, R. *Nat. Mater.* **2006**, *5*, 823–829.

(52) Palkar, V. R.; John, J.; Pinto, R. *Appl. Phys. Lett.* **2002**, *80*, 1628–1630.

(53) Haumont, R.; Kreisel, J.; Bouvier, P.; Hippert, F. *Phys. Rev. B* **2006**, *73*, 132101.

(54) Singh, M. K.; Ryu, S.; Jang, H. M. *Phys. Rev. B* **2005**, *72*, 132101.

(55) Singh, M. K.; Jang, H. M.; Ryu, S.; Jo, M.-H. *Appl. Phys. Lett.* **2006**, *88*, 042907.

(56) Fiebig, M.; Lottermoser, Th.; Kneip, M. K.; Bayer, M. *J. Appl. Phys.* **2006**, *99*, 08E302.

properties. More work is needed to fully understand the finite size effect on spin-phonon coupling and mutual influence of polarization and magnetic ordering in magnetoelectric $BiFeO_3$.

Conclusion

We have presented a comprehensive study of finite-size dependence of crystallographic properties of substrate-free, as-prepared $BiFeO_3$ nanocrystallites. Compared to the prototype ferroelectrics $PbTiO_3$ and $BaTiO_3$, $BiFeO_3$ retains bulk crystallographic dimensions down to a smaller particle size. For crystallites smaller than 30 nm, the crystal structure gradually becomes more symmetric, approaching the ideal, cubic perovskite structure, with increasing unit-cell volume. Extrapolation suggests a critical size of 9 ± 1 nm for the ferroelectric phase. The decrease in Néel temperature with decreasing size has been discussed both in terms of phenomenological scaling relations and possible correlations with the decreasing polarization. High-temperature XRD and differential scanning calorimetry identify the magnetic phase transition to be second-order. Size-dependent polar displacements of cations is an important observation, as it reflects the effect of increasing depolarization field with decreasing crystallite size. Finite size influence on lattice parameters and cation positions show different behavior. The crystallographic measure of polarization, the cooperative, relative displacements of Bi^{3+} and Fe^{3+} quantified by $s - t$, shows a substantial finite value of approximately 75% of bulk even for 13 nm crystallites. Combined with recent observations of increased magnetization of nanoparticles,[19,20] these are promising results with respect to the possibility of making small multiferroic nanostructures for technological applications.

Acknowledgment. Dr. Yingda Yu is acknowledged for performing TEM characterization. This work was supported by the Norwegian University of Science and Technology and the Research Council of Norway (NANOMAT, Grants 158518/431, 140553/I30 and 162874/V00).

Supporting Information Available: XRD patterns, tables, and figures with results from Rietveld refinements (PDF). This material is available free of charge via the Internet at http://pubs.acs.org.

CM071827W